RSC Advances

PAPER

Cite this: *RSC Adv.*, 2016, **6**, 70638

Temperature dependent solubility of gold nanoparticle suspension/solutions

J. A. Powell,[a] R. M. Schwieters,[b] K. W. Bayliff,[a] E. N. Herman,[c] N. J. Hotvedt,[d] J. R. Changstrom,[a] A. Chakrabarti[a] and C. M. Sorensen*[a]

Received 17th June 2016
Accepted 19th July 2016

DOI: 10.1039/c6ra15822f

www.rsc.org/advances

We present measurements of the temperature dependence of thermally reversible solubility for a nanoparticle (NP) suspension/solution. The NPs were gold with an average diameter of 5.5 nm, ligated with dodecanethiol. The solvent was a toluene–dodecanethiol mixture. Analysis of the temperature dependence yielded an enthalpy of dissolution of $\Delta H^{d} = 20.9$ kJ per mole NP. Under the assumption that the NP superlattice solid that dissolves to yield the NP solution is a van der Waals solid, the implied melting temperature was found to be unrealistically high. However, under the same assumption, the minimum of the interparticle potential derived from the data agreed fairly well with a previously presented phenomenological model for the potential. Although the activity coefficient could not be determined due to the lack of a known melting temperature for the NP superlattice solid, any finite melting temperature implied a huge activity coefficient. Scatchard–Hildebrand theory cannot explain the data because the data extrapolate to negative temperatures at a NP mole fraction equal to one. However, the very large activity coefficient was ascribed to the very large molar volume of the NP system, consistent with that theory.

I. Introduction

Nanoparticle colloidal suspensions are currently an area of active research. This is largely due to the fact that it is now possible to synthesize nanoparticles (NPs) with a wide variety of compositions and sizes with narrow size distributions.[1–4] Typically, these NPs are surface ligated so that they are stable against irreversible aggregation.

In this paper we advance the concept that a NP colloidal suspension is a solution with thermally reversible solubility phenomena. We do this by measuring some of its fundamental solution properties. The definition of a solution is simply a homogeneous mixture.[5,6] This description applies well to a NP suspension, especially one with a narrow size distribution. In addition previous work from our lab has shown that, for some NP suspensions, aggregation of the individual NPs can be induced by lowering the temperature and then undone by increasing the temperature;[7,8] *i.e.* the aggregation is thermally reversible. We[9] and others[10,11] have shown that the NP concentration stability limit against aggregation at constant temperature is dependent on both the capping ligand and solvent. We[12] and others[13] have also shown that thermally quenched NP suspensions show nucleation phenomena when the aggregates form. Such thermally reversible, solvent and solute dependent behavior is common to many molecular and ionic solutions.

Given the discussion above, we will take the point of view that a colloidal suspension of NP monomers is a thermally reversible solution as well.[14] A dried precipitate of the NPs is the solute which would dissolve to form a solution of individual NPs (monomers). Like many solutions, the mixture has a phase diagram with single and two-phase regions. In the two-phase region the supernatant is the mixture of single NPs in the solvent; aggregates of single NPs are the solid phase, which settles out under gravity to form the precipitate. Fig. 1, left side, gives a schematic diagram of this NP solution. The equilibrium state is one in which the NP supernatant is in equilibrium with the solid, precipitate phase. The aggregates of the precipitate could have random structures like fractals or be crystalline superlattices.[15] For the ligated gold NPs (AuNPs) suspended (hence dissolved) in an organic phase that we study here, we expect that the NP solution will have some properties similar to non-electrolyte, molecular solutions.

This simple picture, however, is deceptive because the NP monomer is larger and more complex than a common molecule. For example, a 5 nm AuNP would have a significant van der Waals potential, much larger than any organic molecule. The ligand shell is complex. It can undergo phase changes with temperature[16,17] and possibly form patterned structures on the surface of the NP.[10,11] It has become apparent, as recently reviewed,[18] that NPs are different than molecules in that their

[a]*Department of Physics, Kansas State University, Manhattan, KS, 66506, USA. E-mail: sor@phys.ksu.edu*

[b]*Department of Physics and Astronomy, St. Cloud State University, St. Cloud, MN, 56301, USA*

[c]*Department of Physics, St. Norbert College, De Pere, WI, 54115, USA*

[d]*Department of Physics and Astronomy, Iowa State University, Ames, IA, 50011, USA*

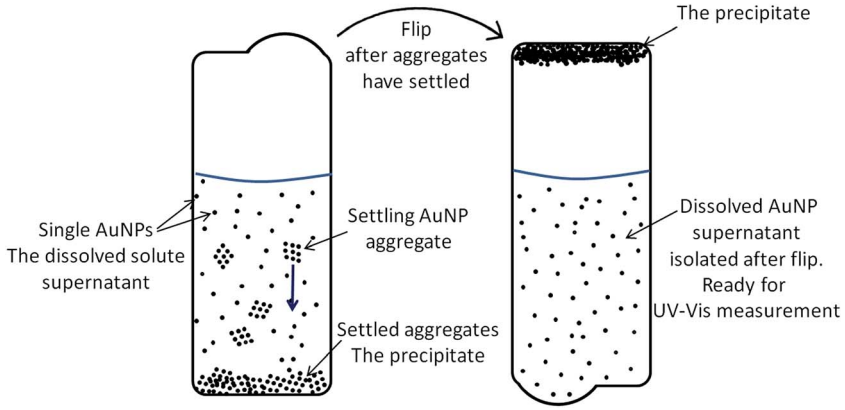

Fig. 1 Diagram showing the nanoparticle solution in the two-phase regime. On the left the dissolved solute of single AuNPs is in equilibrium with aggregates of nanoparticles that settle to form a precipitated solid. The right hand side shows the same system flipped upside down after centrifuging to pellet the precipitate to the bottom of the sealed ampule. This leaves the AuNP supernatant isolated for UV-Vis measurements.

interparticle interactions are not additive and they are internally distinctly inhomogeneous. Furthermore, their size and hence molar volumes are orders of magnitude larger than that of common substances. Lastly, their ligand shells are labile, even at moderate temperatures.

The purpose of this paper is to describe measurements and present data for the saturation solubility of a NP solution as a function of temperature. Specifically, we study the solution properties of 5.5 nm diameter gold nanoparticles with dodecanethiol ligand shells in a solvent of toluene/dodecanethiol of 85/15 mole ratio. From the temperature dependent solubility measurements a numerical determination of the enthalpy of dissolution is obtained and estimates of the activity coefficient are made. Given the lack of knowledge of the properties of the solid phase formed by NPs when they aggregate, and the lack of a theoretical understanding of NP solutions, further interpretation of the data requires some speculation about both. With this caveat, some properties of the inter-particle interaction potential can be determined. However, we find that canonical theoretical descriptions of non-electrolyte solutions cannot provide a complete description of our experimental results.

II. Experimental methods

1. Synthesis

Gold nanoparticles (AuNPs) were synthesized using the toluene–water–dodecyldimethylammonium bromide inverse micelle method followed by digestive ripening as is standard in our lab.[2,15] All chemicals were obtained from Sigma and used as received. 34 mg of gold(III) chloride was dissolved in 10 mL of a 0.02 M solution of dodecyldimethylammonium bromide (DDAB) in toluene. The gold(III) was reduced by adding 40 μL of an aqueous solution of 9.4 M sodium borohydride followed by 30 minutes of stirring. 0.8 mL of 1-dodecanethiol (DDT) was then added to the polydisperse colloid to displace the DDAB and stabilize the colloid followed by 30 minutes of stirring. The amount added was such that the molar ratio of DDT : Au was 30 : 1. The solution of AuNPs was precipitated with 30 mL of ethanol to remove the initial reactants. The precipitated AuNPs were dried under vacuum and redispersed in 10 mL of toluene again with 0.8 mL DDT to maintain a ligand : Au ratio of 30 : 1. The solution was then digestively ripened for 90 minutes under an argon atmosphere. Digestive ripening equilibrates the size distribution to yield a quasi-monodisperse system.

Three synthetic batches were used in the study. Fig. 2 shows a typical TEM picture of the AuNPs synthesized and used in the solubility measurements. Size analysis of these pictures was done by ImageJ with an average of 425 AuNPs evaluated per sample. This analysis determined the average size of the AuNP core in the three batches to be 5.2, 5.5 and 5.8 nm all with 17% standard deviation.

2. Absorption measurements

After digestive ripening, the solution was again precipitated with a threefold excess of ethanol. The supernatant was discarded and the precipitated particles were dried under vacuum and redispersed in a 15% mole fraction solution of DDT in toluene. The redispersed AuNPs were also concentrated by adding less overall solvent than the volume originally precipitated in order to ensure sufficient AuNPs to saturate the

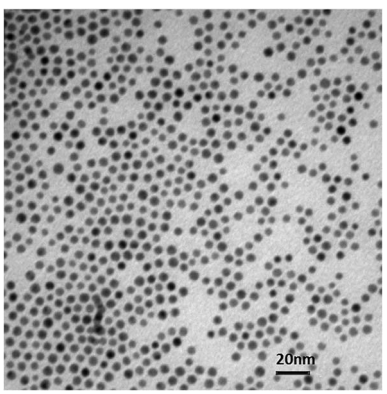

Fig. 2 Transmission electron micrograph of the AuNPs.

solution and create a two-phase system with a saturated supernatant solution in equilibrium with a precipitated solid. Samples of this solution were then placed in clean glass ampules and flame sealed. The ampules had a rectangular cross section of 8 mm by 2 mm and were about 50 mm long. The internal optical path length was 0.8 mm.

With the sample in the two-phase regime, a nanoparticle monomer solution is in equilibrium with precipitated aggregates of monomers. Small, DDT-ligated AuNPs have a plasmon near 524 nm. On the other hand, aggregates of these NPs show a shoulder on this peak towards larger wavelengths. Thus the plasmon can serve two purposes: one is to verify that the supernatant phase contains only monomers and no aggregates, and the other to measure the monomer NP concentration in the supernatant. In our work, UV-Vis absorption spectroscopy was employed for both purposes.

To measure the monomer NP concentration we calibrated the measured UV-Vis absorbance against samples with known gold concentration. Absorption is governed by the Beer–Lambert law

$$I(z) = I(0)\exp(-\tau z) \quad (1)$$

where $I(z)$ is the intensity of light after having passed through a distance z of the solution. The turbidity is $\tau = C_{\text{ext}}n$ where C_{ext} is the extinction cross section and n is the particle number concentration. For particles of a given average size C_{ext} is a constant and for nanoparticles is dominated by the absorption cross section. Commercial UV-Vis spectrometers measure $I(z)$ and $I(0)$ and calculate an absorbance A given by

$$A = \log_{10}[I(0)/I(z)] = 0.43C_{\text{ext}}zn \quad (2)$$

Eqn (2) shows, not surprisingly, that the AuNP supernatant absorbance is directly proportional to AuNP concentration. Two AuNP samples were sent to Gailbraith Laboratories to be analyzed for total gold and were used for AuNP absorbance *versus* concentration calibration. The results from the two samples were consistent. Given the mass concentration of gold in the solution, one can calculate the number of AuNPs per unit volume from the known density of bulk gold, 19.34 g cm^{-3}, and the mean size of the AuNPs, with the assumption that the particles are spherical. This is then converted to mole fraction of AuNPs.

When the AuNP solution is in the two-phase regime, cooling will cause single AuNP to form more aggregates as a precipitate, Fig. 1, left side. Unfortunately, this precipitate is very fine and hence takes a long time to settle out from the supernatant. It was necessary to isolate the supernatant because its concentration was the primary measured quantity. Thus to speed the settling, the experimental apparatus consisted of a modified commercial centrifuge with a home-made temperature-control that allowed for precise temperature regulation of the nanoparticle sample. The centrifuge rotor doubled as the sample holder when taking UV-Vis measurements. This allowed for good sample temperature control as there was very little handling of the glass ampule. UV-Vis spectra were taken on an Ocean Optics 4000+ Spectrophotometer equipped with fiber optic cables.

As stated above, each nanoparticle sample was highly concentrated to ensure a two-phase system consisting of AuNP precipitate (aggregates) in equilibrium with the monomer supernatant. Before the beginning of each run, the sample was sonicated in an ultrasonic bath at room temperature for just long enough to redisperse all of the precipitate, *ca.* 1 minute, but not so much as to affect the temperature. This is a redispersal of the aggregates not a de-aggregation, *i.e.* aggregate dissolution to monomers, that occurs with increasing temperature. The sample ampule was then placed in the centrifuge holder set to a constant temperature. The small volume of sample ($\sim$150 μL) and the small mass of the ampule ensured quick temperature equilibrium to the surrounding aluminum centrifuge rotors. To ensure the two-phase equilibrium of the dissolved AuNP monomers with their aggregates after this handling, the sample was left for 15 minutes at the set temperature. The sample was centrifuged at 7000 rpm (3300g) for 12 minutes to ensure all the aggregates were spun out of the supernatant. Calculation of the barometric height $h = k_{\text{B}}T/mg$ where k_{B} is Boltzmann's constant, T the absolute temperature, m the mass of the particle and g the acceleration in the centrifuge indicate a value of approximately 20 cm for the AuNPs. This indicates they cannot be settled, whereas aggregates a factor of 10 larger have a barometric height of 0.2 cm which indicates complete settling. Upon completion of the centrifugation, the sample was carefully turned upside down to remove the supernatant from the precipitate, as shown in Fig. 1, right side.

Fig. 3 shows an example of the UV-Vis absorbance spectra of the NP supernatant. One can see more absorption at higher temperature indicating more AuNPs dissolved.

The absorbance value at 850 nm was taken as the reference baseline as the solution is transparent at this wavelength. The plasmon peak at around 524 nm was taken as the actual absorbance value. This absorbance is directly proportional to the AuNP supernatant concentration, eqn (2) above. This entire

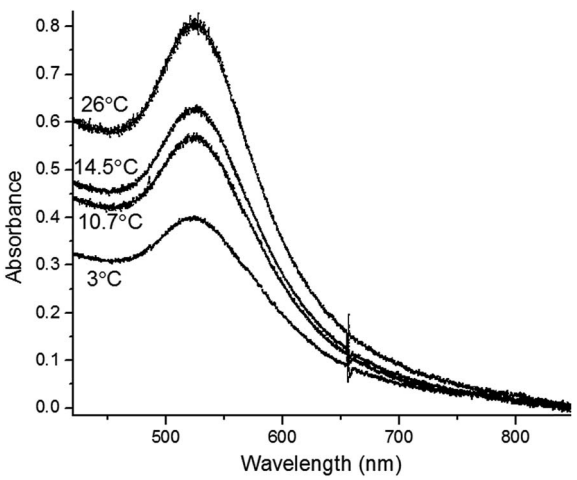

Fig. 3 Measured absorbance as a function of wavelength for an AuNP supernatant in equilibrium with the precipitated solid at four different temperatures. Feature at 660 nm is an equipment artifact.

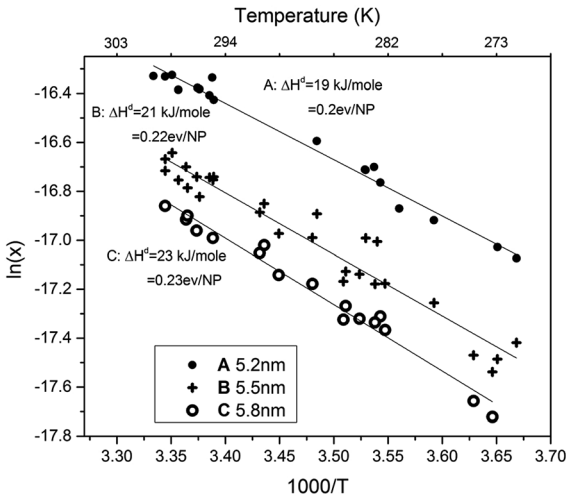

Fig. 4 Log mole fraction of dissolved AuNPs in the supernatant *versus* the inverse temperature for the three samples. Enthalpies of dissolution per mole and per NP are given for each of the three samples.

process was repeated for temperatures ranging from 0° to 30 °C, each time exactly replicating each step to promote reproducibility. This temperature range was chosen for practical purposes. At temperatures above 30 °C, we saw indication of irreversible AuNP aggregation where the increased temperature had detrimental effects on the AuNPs themselves. Temperatures below 0 °C were difficult to maintain with our custom system. There were also problems with condensation of water vapor at low temperatures on the glass ampules impeding reproducible measurements with the UV-Vis.

In summary, the absorbance of the equilibrium supernatant of the AuNP solution was measured as a function of temperature, T. This absorbance was converted to mole fraction AuNPs, x, and ln x is plotted *versus* $1/T$ in Fig. 4.

III. Results and analysis

1. The enthalpy of dissolution

According to thermodynamic theory,[19] the solid phase-dissolved phase equilibrium solute mole fraction x at a temperature T is given by

$$\ln x = -\frac{\Delta H^{\mathrm{d}}}{R}\left(\frac{1}{T}-\frac{1}{T_{\mathrm{m}}}\right) - \ln \gamma \qquad (3)$$

where T_{m} is the solid phase solute melting temperature, γ is the activity coefficient for the dissolved solute and R is the ideal gas constant. Eqn (3) also claims that the enthalpy of dissolution is equal to the enthalpy of fusion, $\Delta H^{\mathrm{d}} = \Delta H^{\mathrm{f}}$, of the solute. Given eqn (3), the solubility data were plotted ln x *versus* $1/T$ as shown in Fig. 4. From fitting the three data sets to eqn (3) we find the enthalpies of dissolution of the three samples to be endothermic with values of 19.1 kJ per mole NP, 22.6 kJ per mole NP and 20.9 kJ per mole NP for an average of 20.9 per mole NP.

Little is known about the NP solid that forms upon precipitation from solution and hence stands in equilibrium with the dissolved supernatant. This fact and the novelty of our data lead us to try various scenarios in an attempt to find an adequate explanation of the data.

For the NP solid numerous examples exist of superlattice formation with twelve-fold coordination.[15] Given the roughly spherical nature of the NPs, their lack of significant charge if one assumes that they are identical, and the van der Waals force that exists between the NPs when they are far apart, one can, to lowest order, envision a van der Waals solid similar to those formed by the inert gases. For argon the lattice cohesive energy is a factor of 6.5 larger than the latent heat of fusion; similar values exist for the other inert gases.[20] Then with this analogy, the NP lattice cohesive energy is 6.5 times larger than the enthalpy of dissolution to imply $U_{\mathrm{coh}} = 136$ kJ per mole NP. It is an empirical fact that the melting temperature of the inert gas solids is well described by $T_{\mathrm{m}} = U_{\mathrm{coh}}/103$ (J mol^{-1} K^{-1}); hence we predict $T_{\mathrm{m}} = 1300$ K for a van der Waals solid of NPs. This seems rather large to imply that the van der Waals solid hypothesis is weak from this perspective.

In previous work we developed a phenomenological nanoparticle–nanoparticle pair potential for alkane thiol ligated gold NPs.[21] The potential included van der Waals interactions between the gold cores. It treated the ligands as elastic, flexible polymer chains hence the potential had contributions from compression of the ligands and the free energy of mixing of the chains with themselves. In a slightly different approach the pair potential involved a possible situation in which the ligand layers are compressed without any interpenetration when two NPs are in close contact. This conformation is known as "denting".[22] The separation of the NPs at the potential minimum compared well with experimental results of AuNP superlattice constants for various ligand lengths. Fig. 5 shows the results of our model for AuNPs ligated with dodecanethiol with and without denting.

Fig. 5 shows the minimum potentials are $\varepsilon = -0.10$ eV and -0.13 eV for ligand mixing and ligand denting potentials, respectively. We again follow the analogy to van der Waals solids and assume that the NP superlattice cohesive energy is

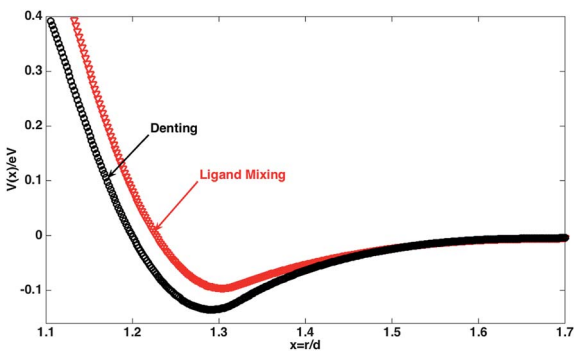

Fig. 5 Nanoparticle interparticle potential $V(x)$ in electron volts *versus* nanoparticle center to center separation r divided by the nanoparticle diameter d for $d = 5.5$ nm AuNPs with a dodecanethiol ligand shell. The solid lines are effective potentials with contributions from van der Waals, ligand mixing with and without compression, and elastic compression terms. Symbols are for the effective potentials where the ligand mixing parts of the effective potential have been replaced by the denting potential.

related to the interparticle potential minimum ε by the same formula that relates the van der Waals solid total lattice cohesive energy, $U_{coh} = 8.6N\varepsilon$, where N is the total number of atoms or NPs.[20] Then using the NP superlattice energy, $U_{coh} = 136$ kJ per mole NP, derived above from the measured enthalpies of dissolution under the van der Waals solid assumption, we find an experimental value of $\varepsilon = -0.165$ eV. This compares favorably to the values from the phenomenological model, especially given all the assumptions involved. In summary, the van der Waals solid model was not successful for estimating the melting temperature, but shows modest agreement with the interparticle potential well minimum. We do not have a hypothesis for why this is so.

Returning to Fig. 4, note that the enthalpies of dissolution of the three samples show an increase of about 10% as the gold core diameters of the AuNPs increase also by about 10%. Caution is warranted with this trend, however, because the uncertainties in both the measured enthalpies and core diameters are also about 10%. Nevertheless, one would expect that larger metallic cores would lead to stronger van der Waals interactions which would then lead to larger enthalpies of dissolution, consistent with this possible trend.

2. The activity coefficient

Replotting the data of Fig. 4 on an expanded scale in Fig. 6 shows that the nanoparticles have a very non-ideal solution behavior. In an ideal solution the $\ln x = 0$ intercept would occur at the solute melting temperature, T_m. The collective data from all three samples in Fig. 6 extrapolate to negative temperature. The intercepts of eqn (3) at $1/T = 0$ and $\ln x = 0$ yield the same relation between $\ln \gamma$ and T_m. Given the large scale of Fig. 6 compared to the scale of the data, the relation is only good to one significant figure. Nevertheless, it is useful. It is

$$\ln \gamma = 8 + 2500/T_m \quad (4)$$

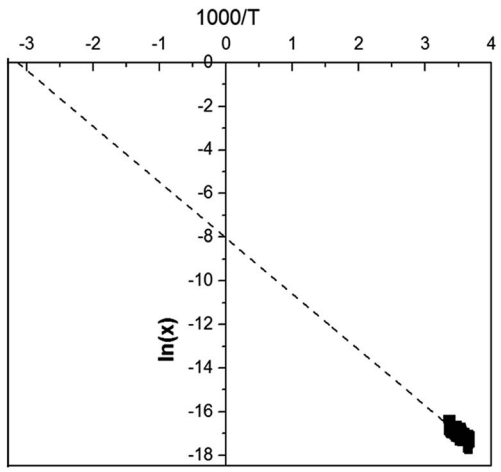

Fig. 6 Log mole fraction of AuNPs *versus* the inverse temperature on a larger scale than Fig. 3 for the aggregate data (lower right corner) of all three runs of solubility measurements.

Unfortunately, this is one equation with two unknowns, and we have no way to measure either of these two unknowns independently. Previous attempts to measure the melting point of the NP solid (*i.e.* the aggregated solid of NPs, not the NPs themselves) in our lab [unpublished] indicated $T_m \simeq 120$ °C, but the results were poorly reproduced because the NP with its ligand shell decomposed at high temperature. Regardless, if we make a reasonable guess that $T_m = 400$ K, then an activity coefficient of $\gamma = 1.4 \times 10^6$ is obtained, a very large value. If we use the van der Waals solid inferred value of $T_m = 1300$, then $\gamma = 1.8 \times 10^5$. Indeed, if we use $T \rightarrow \infty$, $\gamma = 2700$. We conclude that the activity coefficient is very large.

Scatchard–Hildebrand theory can be used to calculate the activity coefficient for regular solutions which are defined as those for which there is no excess entropy of mixing (the entropy of mixing is the same as for an ideal solution). Regular solution theory applies for solute and solvent being similar, which is certainly not the case for NPs and a molecular solvent. Nevertheless, lacking any other theoretical framework, we proceed. The activity coefficient for the solute is predicted to be[19]

$$RT \ln \gamma = v\Phi_{solv}^2(\delta - \delta_{solv})^2 \quad (5)$$

where v is the molar volume of the solute, Φ_{solv} is the volume fraction of the solvent and δ and δ_{solv} represent the solubility parameters of the solute and solvent, respectively. The expected failure of Scatchard–Hildebrand theory for the NP solution appears most notably in the temperature dependence in eqn (5). When eqn (5) is substituted into eqn (3), the result will not allow for a negative temperature extrapolation which the data so strongly show in Fig. 5. However, eqn (5) does hint to the origin of the very large activity coefficient because the molar volume of the NP is huge, approximately $v \simeq 160$ liters (assuming a Au core plus ligand shell for a total diameter of 8 nm). We ask: how could one possibly have an equal molar solution, *i.e.* $x = 1/2$ of nanoparticles when the molar volume of the solvent is *ca.* 0.1 liter? From a different perspective, if equal volumes of toluene and NP were mixed, the mole fraction of NP would be $x = 6.6 \times 10^{-4}$.

IV. Conclusions

We have presented what appear to be the first measurements of the temperature dependence of thermally reversible solubility for a nanoparticle suspension/solution. Analysis with standard thermodynamic solution theory yields an enthalpy of dissolution of $\Delta H^d = 20.9$ kJ per mole NP for AuNPs ligated with dodecanethiol with an average core gold diameter of 5.5 nm. Under the assumption that the NP superlattice solid that dissolves to yield the NP solution is a van der Waals solid, the implied melting temperature is unrealistically high. However, under the same assumption, the minimum of the interparticle potential derived from the data agreed fairly well with a previously presented phenomenological model for the potential. The activity coefficient could not be determined due to the lack of a known melting temperature for the NP superlattice solid. However, any finite melting temperature implied a huge activity

coefficient, consistent with the fact that the thermodynamic analysis extrapolated to negative temperature at NP mole fraction equal one. Attempts to apply Scatchard–Hildebrand theory failed. However, the very large activity coefficient was ascribed to the very large molar volume of the NP system, consistent with that theory. It appears that our data indicate the need for a new theoretical framework to describe nanoparticle solutions.

References

1 M. Brust, M. Walker, D. Bethell, D. J. Schiffrin and R. Whyman, *Chem. Commun.*, 1994, **7**, 801.

2 X. M. Lin, C. M. Sorensen and K. J. Klabunde, *J. Nanopart. Res.*, 2000, **2**, 157.

3 K. J. Klabunde, *Nanoscale Materials in Chemistry*, Wiley Interscience, New York, 2001.

4 M.-C. Daniel and D. Astruc, *Chem. Rev.*, 2004, **104**, 293.

5 L. Pauling, *General Chemistry*, Dover, New York, 1970.

6 E. A. Moelwyn-Hughes, *Physical Chemistry*, Pergamon, Oxford, 1961.

7 X. M. Lin, G. M. Wang, C. M. Sorensen and K. J. Klabunde, *J. Phys. Chem. B*, 1999, **103**, 5488.

8 B. L. V. Prasad, S. I. Stoeva, C. M. Sorensen and K. J. Klabunde, *Langmuir*, 2002, **18**, 7515.

9 B. C. Lohman, J. A. Powell, S. Cingarapu, C. B. Aakeroy, A. Chakrabarti, K. J. Klabunde, B. M. Law and C. M. Sorensen, *Phys. Chem. Chem. Phys.*, 2012, **14**, 6502.

10 A. Centrone, E. Penzo, M. Sharma, J. W. Myerson, A. M. Jackson, N. Marzari and F. Stellacci, *Proc. Natl. Acad. Sci. U. S. A.*, 1998, **105**, 9886.

11 O. Uzun, Y. Hu, A. Verma, S. Chen, A. Centrone and F. Stellacci, *Chem. Commun.*, 2008, 196.

12 H. Yan, S. Cingarapu, K. J. Klabunde, A. Chakrabarti and C. M. Sorensen, *Phys. Rev. Lett.*, 2009, **102**, 095501.

13 O. C. Compton and F. E. Osterloh, *J. Am. Chem. Soc.*, 2007, **129**, 7793.

14 C. M. Sorensen, in *Nanoscale Materials in Chemistry: Environmental Applications*, ed. L. E. Erickson, R. Koodali and R. Richards, ACS Symp. Ser, 2010, vol. 1045, pp. 35–49.

15 B. L. V. Prasad, C. M. Sorensen and K. J. Klabunde, *Chem. Soc. Rev.*, 2008, **37**, 1871.

16 W. D. Luedtke and U. Landman, *J. Phys. Chem.*, 1996, **100**, 13323.

17 Y. Yu, A. Jain, A. Guillaussier, V. R. Voggu, T. M. Truskett, D.-M. Smilgiesb and B. A. Korgel, *Faraday Discuss.*, 2015, **181**, 181.

18 C. A. Silvera Batista, R. G. Larson and N. A. Kotov, *Science*, 2015, **350**, 1242477.

19 J. M. Prausnitz, R. N. Lichtenthaler and E. Gomez de Azevedo, *Molecular Thermodynamics of Fluid-Phase Equilibria*, Prentice Hall, Englewood Cliffs, NJ, 1986.

20 C. Kittel, *Introduction to Solid State Physics*, Wiley, New York, 2005.

21 S. J. Khan, F. Pierce, C. M. Sorensen and A. Chakrabarti, *Langmuir*, 2009, **25**, 13861.

22 J. B. Smitham, R. Evans and D. H. Napper, *J. Chem. Soc., Faraday Trans.*, 1975, **71**, 285.